AIChE

An Improved Model for Boron Diffusion and Activation in Silicon

Charlotte T. M. Kwok and Richard D. Braatz
Dept. of Chemical and Biomolecular Engineering, University of Illinois, Urbana, IL 61801

Silke Paul and Wilfried Lerch
Mattson Thermal Products GmbH, Daimlerstrasse 10, 89160 Dornstadt, Germany

Edmund G. Seebauer
Dept. of Chemical and Biomolecular Engineering, University of Illinois, Urbana, IL 61801

DOI 10.1002/aic.11984
Published online September 29, 2009 in Wiley InterScience (www.interscience.wiley.com).

Technologies such as solid-phase epitaxial regrowth and millisecond annealing techniques have led to a wide range of maximum temperatures and heating rates for activating dopants and eliminating ion implantation damage for transistor junction formation. Developing suitable annealing strategies depends on mathematical models that incorporate accurate defect physics. The present work describes a model that includes a newly discovered representation of defect annihilation at surfaces and of near-surface band bending, together with an improved representation of interstitial clustering. Key parameters are determined by maximum likelihood (ML) estimation and maximum a posteriori (MAP) estimation. The model yields a substantially improved ability to model the behavior of implanted boron over a wide range of annealing conditions.
 AIChE J, 56: 515–521, 2010
Keywords: semiconductor defects, annealing, interfaces, silicon, diffusion

Introduction

The stringent scaling requirements on transistor junction depth and dopant activation outlined by the International Technology Roadmap for Semiconductors[1] have given rise to annealing methods after ion implantation that span a vast array of time scales. These scales range from several minutes for solid-phase epitaxial regrowth[2] to about one second for ''spike'' annealing based on incandescent lamps[3] to about 1 ms for methods based on flashlamps[4] and lasers.[5] Empirical data suggests that shorter time scales reduce dopant diffusion and increase activation.[6] However, the complicated defect dynamics that govern diffusion and activation make the physical mechanism difficult to understand and fully exploit. Indeed, the benefits of combining different annealing methods into a single process flow,[7] the effects of peak temperature,[8] and the effects of preheating prior to the main annealing step pulse[8] all require better explanation.

The development of suitable annealing strategies depends heavily on mathematical models that incorporate accurate rate expressions for key elementary steps in the defect physics. In the case of boron implanted into silicon, this laboratory has discovered new ways in which a surface can influence diffusion and activation through an electrostatic mechanism[9] and an exchange mechanism of interstitials with surface dangling bonds.[10] The electrostatic mechanism describes the effects on charged interstitials of near-surface band bending, which results from surface bond rupture during implantation. The exchange mechanism accounts for the effects of surface dangling bond concentration on the rate of interstitial annihilation. This work incorporates these effects through a systems-based approach involving maximum likelihood (ML) estimation and maximum a posteriori (MAP) estimation. These methods provide mathematically rigorous

Correspondence concerning this article should be addressed to E. G. Seebauer at eseebaue@illinois.edu

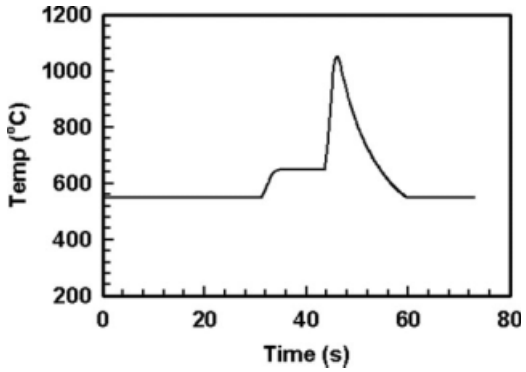

Figure 1. Temperature trajectory for spike annealing with a peak temperature of 1050°C.

means for estimating parameters for individual elementary steps in complex diffusion-reaction networks without arbitrary curve fitting. The model captures the behavior of dopant diffusion and activation over a fairly wide range of annealing temperatures and times.

Experimental Methods

This work employed data for the diffusion and activation of implanted boron in two time regimes: many minutes (''soak'' annealing) and about 1 s (spike annealing). Soak annealing experiments utilized n-type prime Si (100) wafers implanted with boron at 2 kV and a dose of 1×10^{15} ions/cm^2 (implantation done at Varian). The annealing step was performed as described previously[11] in a turbomolecularly pumped ultrahigh vacuum chamber with a base pressure in the low 10^{-8} torr range. Specimens of approximate dimensions of 2 cm $\times$ 2 cm were cut from the wafers and mounted in the vacuum chamber using Ta clips for resistive heating. Temperature was monitored with a chromel-alumel thermocouple junction pressed into a small pit drilled into the silicon. Samples were annealed at 900°C for 1 h.

Spike annealing data were obtained at Mattson Thermal Products GmbH, with details described in Ref. 12. In brief, n-type prime (100) Si wafers were implanted with boron at 0.5 kV to a dose of 1×10^{15} ions/cm^2. The surface was prepared differently from the soak anneal experiments. Before implantation, the native oxide was removed by wet-chemical etching in HF (49%):H_2O solution. Annealing was performed in a Mattson rapid thermal processing (RTP) system with a temperature trajectory (Figure 1) having a maximum temperature of 1000 and 1050°C. The gaseous ambient was N_2 with 100 ppm partial pressure of O_2.

Characterization of soak-annealed samples was performed at the University of Illinois. Profiles were measured ex situ by secondary ion mass spectroscopy (SIMS) using a CAMECA IMS-5f instrument. Sheet resistance was measured by a standard four-point probe. The spike-annealed samples were analyzed at Mattson, with profiles measured ex situ by SIMS on a FEI SIMS 4600 quadrupole depth profiler. For dopant activation, full-wafer sheet resistance mapping was performed by a KLA Tencor RS100.

Model Formulation

The boron diffusion model originated from an earlier version based on spike annealing experiments.[13] However, that model had limited ability to predict behavior at widely differing time scales and temperatures.[14] This model was implemented by the profile simulator FLOOPS 2000.[15] Briefly, the model utilizes continuum equations to describe the reaction and diffusion of boron interstitial atoms and related defects in silicon. These equations have the general form for species i:

$$\frac{\partial C_i}{\partial t} = -\frac{\partial J_i}{\partial x} + G_i \tag{1}$$

where C_i, J_i, and G_i denote the concentration, flux, and net generation rate of species i, respectively. The flux J_i consists of Fickian diffusion and electric drift motion. The net generation G_i incorporates terms associated with formation and dissociation of interstitial clusters and kick-in/kick-out reactions between interstitials and the lattice through the formation of a boron-interstitial complex:

$$\mathrm{B}_s + \mathrm{Si}_i \underset{k_{\mathrm{dis}}}{\overset{k_{\mathrm{assoc,B}}}{\rightleftarrows}} (\mathrm{B}_s - \mathrm{Si}_i) \underset{k_{ki}}{\overset{k_{ko}}{\rightleftarrows}} \mathrm{B}_i + \mathrm{Si}_s \tag{2}$$

Three significant improvements have been made to the set of rate expressions in the model.

The first improvement involved incorporating a more accurate description of the effects of surface annihilation of boron and silicon interstitials. The previous version of the simulator used for parameter estimation assumed that the surface acts as a perfect reflector for interstitials. In fact, there exists both computational[16,17] and experimental evidence[18–20] that the Si surface or Si/SiO_2 interface is capable of removing interstitials. Such ability is also well characterized for the metal-alloy/Si interface. For example, Lerch et al.[21] has measured the effectiveness of the metal-alloy/Si interface as a sink for self-interstitials for gold diffusion in silicon. Recently, this laboratory has quantified the annihilation rate for Si interstitials at the Si(100) surface and has shown for implanted isotopically labeled silicon,[10] boron,[22] and arsenic[23] that the surface can act as a controllable sink for interstitials by adjusting the degree of surface dangling bond saturation. Because silicon interstitials enhance the diffusion of boron by the kick-out reaction, the perfect reflector assumption is likely to overestimate the degree of profile spreading. Moreover, this effect is more pronounced for lower ramp-rates because of the longer time for interstitial liberation from clusters and for interstitials to escape to the surface. This assumption is also linked to the lack of profile fit in the region close to the surface (<15 nm).[13] To incorporate a more accurate description for interstitial annihilation at surface, the model boundary condition for interstitials is modified to

$$-D_k \left.\frac{\partial C_k}{\partial x}\right|_{x=0} = J_{\mathrm{total},k} S_k, \tag{3}$$

where $k = \mathrm{Si}_i$, B_i, $J_{\mathrm{total},k}$ denotes the total impinging flux of interstitials, and S_{B_i} and S_{Si_i} are the surface loss probabilities[24] of boron and silicon interstitials, respectively. The surface loss probability quantifies the effectiveness of the surface in removing boron and silicon interstitials. The actual flux at the

surface is the product of the total impinging flux and the surface loss probability. For the present simulation, S_{Si_i} and S_{B_i} are assumed to be equal; however, it is conceivable that dopant and silicon interstitials have different annihilation probabilities at the surface. The value was set at 2.5×10^{-5}, based on experimental data obtained elsewhere.[25]

The second improvement involved incorporation of the effects of near-surface band bending. Previous modeling of boron diffusion assumes no Fermi-level pinning at the surface and no corresponding near-surface band bending. Photoreflectance measurements have shown experimentally[26] that sub-kV ion bombardment leads to near-surface band bending (both for an atomically clean silicon surface and the silicon-oxide interface). The band bending at the oxide interface results from electrically active defects created by implantation-induced bond rupture. This band bending creates a near-surface electric field that largely opposes the motion of charged interstitials toward the surface. The effective surface boundary condition for point defect annihilation therefore changes, which in turn alters the concentration of such defects in the underlying bulk. Model predictions[9] show that surface band bending can significantly deepen dopant junction by repelling positively charged interstitials. These surface defects responsible for band bending can be eliminated, but only with annealing at fairly high temperatures for several minutes. For example, experimental results[26] indicate that at 940°C, it takes roughly 5 min to heal the electrically active defects. The temperature dependence of the healing kinetics is weak. Thus, for a spike anneal in the presence of native oxide, surface band bending persists throughout the heating cycle because the surface is exposed to high temperatures (>800°C) for at most a few seconds (Figure 1). However, a corresponding soak anneal at 900°C for 60 min would lead to little band bending for most of the heating cycle. Thus, the present simulations incorporate near-surface band bending for the spike anneal but not the soak anneal. Where band bending is included, the position of the surface Fermi level is fixed at 39 kJ/mol (0.4 eV) above the valance band, in accord with the experimental value.[26]

The third improvement involved increasing the maximum size of the interstitial clusters from five to eight. In actual implanted silicon, the cluster size can increase without limit to form well-known {311}-defects, although the FLOOPS simulator can handle only a limited number of mass balance equations for the defect species. The consequences have been addressed previously for the case of silicon self-diffusion[27] and can include premature dissociation of clusters in the simulation and discrete bursts of dissociation as the temperature rises. Premature dissolution of large clusters can be avoided by equating the dissociation energy for the largest clusters in the simulation to that for very large clusters in actual Si. This approach works because the dissociation energies of all clusters above about 15 atoms in Si[28] are the same. Because the dissociation energy of clusters in Si generally decreases below about 15 atoms, the corresponding energies in the simulator are spread evenly in proportion (in accord with the spirit of ML analysis). With a five-atom maximum on cluster size, however, this approach leads to a wide discretization of dissociation energies that causes unnaturally large bursts of dissociation at a few specific temperatures. Increasing the maximum size to eight atoms greatly reduces the discretization and more closely approximates the actual physical system. In this implementation, the model consists of 40 highly stiff coupled partial differential equations (including Poisson's equation). The reactions for the clustering of interstitials for pure Si and mixed B–Si clusters are

$$B_nSi_{m-1} + Si_i \underset{k_{disso}}{\overset{k_{assoc,Si}}{\rightleftarrows}} B_nSi_m \tag{4}$$

$$B_{n-1}Si_m + B_i \underset{k_{disso}}{\overset{k_{assoc,B}}{\rightleftarrows}} B_nSi_m, n+m \leq 8, \tag{5}$$

where the index of m and n denote the number of silicon and boron interstitials in the cluster, respectively.

The initial condition for each simulation run was an experimental as-implanted boron profile. Controversy exists for the percentage of substitutional boron just after implantation. For example, Caturla et al.[29] and Kobayashi et al.[30] have suggested that 20% of the implanted boron enters substitutional sites. However, recent KMC simulations by Pelaz et al.[31] showed that only ~3% of implanted boron enters substitutional sites and that the rest enter mixed B–Si interstitial clusters. Fortunately, sensitivity analysis using the present model showed that the results are largely independent of the initial amount of substitutional boron. Variation of the initial substitutional percentage over the range of 2–20% resulted in profile changes smaller than the measurement error in SIMS. This work assumes that 20% of implanted boron enters substitutional sites, mainly to keep it consistent with previous simulation studies.[13] However, this assumption should be taken with caution and verified by sensitivity analysis in the future when different implant or annealing conditions are employed. The initial condition for silicon interstitial was set based on the "+1 model"[32] in which its concentration exactly tracks the local concentration of implanted boron.

Key reaction expressions and rate parameter definitions are summarized in Table 1. Energetics for steps involving mixed Si–B clustering, boron diffusion, and activation have been determined previously by maximum likelihood (ML) estimation and maximum a posteriori (MAP)[13] estimation utilizing results from density functional theory calculations, experiments for certain elementary steps reported in the literature, and previous experiments on spike annealing of boron. Parameters connected with self-interstitial diffusion and the dissociation of pure Si clusters have been further refined[27] utilizing additional information from silicon self-diffusion experiments. Despite the increase of the maximum cluster size from five to eight, the largest cluster plays the same role as the corresponding cluster in previous work. The numerical values of the parameters for the largest clusters have been estimated previously by ML estimation and MAP estimation.[27]

For cluster sizes of three through seven, estimates were obtained by linear interpolation between the end points of sizes two and eight. This approach contrasts with literature[28,33–36] that reports a non-monotonic progression of cluster dissociation energy with increasing size; for example, minima appear at sizes of roughly four and eight atoms. However, the interpolation follows the spirit of maximum likelihood estimation.[37] More importantly, accurate simulation of the phenomena examined here does not depend on

Table 1. Key Reactions Expressions and Rate Parameter Definitions in the Boron Diffusion Model

Reactions	Equations and Rate Constants
1. Interstitial diffusion	
Silicon	$D_{\mathrm{Si}} = A_{\mathrm{diff}} \exp(-E_{\mathrm{diff,Si}}/kT)$
Boron	$D_{\mathrm{B}} = A_{\mathrm{diff}} \exp(-E_{\mathrm{diff,B}}/kT)$
2. Kick-in/kick-out reaction	$\mathrm{B}_s + \mathrm{Si}_i \underset{k_{\mathrm{dis}}}{\overset{k_{\mathrm{assoc,B}}}{\rightleftarrows}} (\mathrm{B}_s{-}\mathrm{Si}_i) \underset{k_{\mathrm{ki}}}{\overset{k_{\mathrm{ko}}}{\rightleftarrows}} \mathrm{B}_i + \mathrm{Si}_s$
	$k_{\mathrm{assoc,B}} = 4\pi a D^*_{\mathrm{B}}$
	$k_{\mathrm{ko}} = A_{\mathrm{ki/ko}} \exp(-E_{\mathrm{ko}}/kT)$
	$k_{\mathrm{ki}} = A_{\mathrm{ki/ko}} \exp(-E_{\mathrm{ki}}/kT)$
	$k_{\mathrm{dis}} = A_{\mathrm{ki/ko}} \exp(-E_{\mathrm{dis}}/kT)$
3. Cluster dissociation	
Pure Si cluster	$\mathrm{Si}_m \rightarrow \mathrm{Si}_{m-1} + \mathrm{Si}_i (m = \text{size of Si cluster})$
	$k_{\mathrm{disso,Si}} = A_{\mathrm{disso}} \exp(-E_m/kT)$
Pure B cluster	$\mathrm{B}_n \rightarrow \mathrm{B}_{n-1} + \mathrm{B}_i (n = \text{size of B cluster})$
	$k_{\mathrm{disso,B}} = A_{\mathrm{disso}} \exp(-E_{n,\mathrm{B}}/kT)$
Mixed B–Si cluster	$\mathrm{B}_n\mathrm{Si}_m \rightarrow \mathrm{B}_n\mathrm{Si}_{m-1} + \mathrm{Si}_i$
	$\mathrm{B}_n\mathrm{Si}_m \rightarrow \mathrm{B}_{n-1}\mathrm{Si}_m + \mathrm{B}_i$
	$k_{\mathrm{disso,mix}} = A_{\mathrm{disso}} \exp(-E_{(n+m),\mathrm{mix}}/kT)$
4. Cluster association	
Si interstitial	$\mathrm{B}_n\mathrm{Si}_{m-1} + \mathrm{Si}_i \rightarrow \mathrm{B}_n\mathrm{Si}_{\mathrm{m}}$
	$\mathrm{Si}_{m-1} + \mathrm{Si}_i \rightarrow \mathrm{Si}_m$
	$k_{\mathrm{assoc,Si}} = 54\pi a D^*_{\mathrm{Si}}$
B interstitial	$\mathrm{B}_{n-1}\mathrm{Si}_m + \mathrm{B}_i \rightarrow \mathrm{B}_n\mathrm{Si}_m$
	$\mathrm{B}_{n-1} + \mathrm{B}_i \rightarrow \mathrm{B}_n$
5. Surface annihilation	$k_{\mathrm{assoc,B}} = 4\pi a D^*_{\mathrm{B}}$
Si interstitial	$-D_{\mathrm{Si}} \frac{\partial C_{\mathrm{Si}_i}}{\partial x}\Big\|_{x=0} = J_{\text{total, Si}_i} S_{\mathrm{Si}_i}$
B interstitial	$-D_{\mathrm{B}} \frac{\partial C_{\mathrm{B}_i}}{\partial x}\Big\|_{x=0} = J_{\text{total, B}_i} S_{\mathrm{B}_i}$

a = capture radius for cluster association [13].

the details of the cluster dissociation energies assumed for intermediate cluster sizes. Formal sensitivity analysis shows this effect quantitatively;[37] the dissociation energies of intermediate clusters exert relatively little effect. The reason can be explained as follows. When dissociation energies increase monotonically with cluster size (or even loosely so), dissociating one atom from a cluster sets off a rapid cascade of further dissociation events that quickly liberates all the interstitials in the cluster. The details of those further dissociation events do not matter very much because those steps all occur rapidly compared with the initial step. For this reason, this model also makes the simplifying assumption that the dissociation energy of mixed Si–B clusters depends only on the total number of atoms, e.g., $E_{\mathrm{B_2SI3}} = E_{\mathrm{B_3SI2}}$. However, the model does distinguish between mixed clusters and pure Si clusters. The differences in dissociation energies between mixed and pure clusters are generally modest but become more pronounced as the clusters approach the next-to-largest permissible size. This effect correlates with the increase in model sensitivity coefficients in this regime and reflects the fact that in most experiments, the clusters just below the largest size are typically most active in the initial dissociation cascade.[37]

This model was used in conjunction with MAP estimation, which determines the most likely values of parameters when prior information is already available.[38,39] MAP estimation optimally combines prior statistical information of the parameter estimates with additional experimental data to obtain improved a posteriori estimates. For this application, MAP estimation can be equivalently posed as a minimization problem

$$\min_{\substack{\beta \\ j=1,\cdots,d}} \left\{ (\overline{\beta} - \mu)^T V_\mu^{-1} (\overline{\beta} - \mu) + \sum_{j=1}^{d} \left(Y_j - P_j(\overline{\beta}, S_j)\right)^T V_{\varepsilon j}^{-1} \left(Y_j - P_j(\overline{\beta}, S_j)\right) \right\} \quad (6)$$

where $\overline{\beta}$ denotes the vector of estimated parameters that are the same for all profiles, μ is the vector of corresponding a priori parameter estimates, V_μ is the prior parameter covariance matrix, d is the total number of SIMS profiles, S_j is the surface loss probability, Y_j is the vector of experimental observations, P_j is the vector of model predictions, and $V_{\varepsilon,j}$ is the measurement covariance matrix for the jth profile that has been estimated previously [Ref. 24] by the measurement of different SIMS profiles on the same sample.

The a priori information available for many of the parameters originated from earlier application of ML estimation to this problem.[13,27] The ML approach[38] gives the most likely value for each parameter based on the available literature, which typically employs density functional theory calculations or specific experiments. The ML approach also estimates the corresponding uncertainty. The most likely value $\overline{y}$ for a given parameter is obtained by minimizing the objective function:

$$\Phi(\overline{y}) = \sum_i w_i (y_i - \overline{y})^2, \quad (7)$$

where y_i denotes the estimate for the parameter drawn from a particular source i in the literature, and w_i is a weighting factor that accounts for the accuracy of y_i. Setting the derivative of $\Phi(\overline{y})$ with respect to $\overline{y}$ equal to zero yields an analytic formula for $\overline{y}$:

$$\overline{y} = \frac{\sum_i w_i y_i}{\sum_i w_i}. \quad (8)$$

Results and Discussion

Table 2 shows the ML/MAP estimates and the associated standard deviation of the model parameters. Figures 2 and 3 show sample simulation results of the eight-atom model that employs ML/MAP values of the parameters. The modifications in cluster dissociation energies, surface boundary condition for interstitials, and near-surface band bending lead to good agreement between the simulated and experimental spike and soak annealed profiles. By contrast, the previous model poorly captured boron diffusion profiles at low ramp rates[14] (and presumably even more poorly for constant-temperature soak annealing). Note that the present parameter set involves no arbitrarily adjustable parameters; all parameters were obtained from specific experiments aimed at the relevant elementary steps or through rigorous ML/MAP analysis.

The two model modifications involving the surface play crucial roles in correctly capturing the interplay of boron with the surface and the implant-induced defects. It is important to include each modification separately and not to lump them together into an "effective" surface annihilation probability. Such an approach may work in certain restricted cases; indeed, a simple perfect reflector boundary condition has been employed with success under some conditions.[40,41]

Table 2. Model Parameters and ML/ MAP Estimates

Parameters	Unit	Value	Standard deviation	Method	References
1. Cluster dissociation—pure silicon cluster					
E_2 (size 2)	kJ/mol	134.9	2.9	ML	13
E_3 (size 3)	kJ/mol	173.1	*	*	*
E_4 (size 4)	kJ/mol	211.2	*	*	*
E_5 (size 5)	kJ/mol	249.4	*	*	*
E_6 (size 6)	kJ/mol	287.5	*	*	*
E_7 (size 7)	kJ/mol	325.6	*	*	*
E_8=E_{large} (large)	kJ/mol	363.8	0.29	MAP	27
2. Cluster dissociation—pure boron cluster					
$E_{2,\text{B}}$ (size 2)	kJ/mol	172.3	1.2	MAP	13
3. Cluster dissociation—mixed B–Si cluster					
$E_{3,\text{mix}}$ (size 3)	kJ/mol	168.6	*	*	*
$E_{4,\text{mix}}$ (size 4)	kJ/mol	202.4	*	*	*
$E_{5,\text{mix}}$ (size 5)	kJ/mol	236.1	*	*	*
$E_{6,\text{mix}}$ (size 6)	kJ/mol	269.8	*	*	*
$E_{7,\text{mix}}$ (size 7)	kJ/mol	303.6	*	*	*
$E_{8,\text{mix}} = E_{\text{large,mix}}$ (large)	kJ/mol	337.2	#	ML	13
4. Kick-in/kick-out reaction					
E_{ko}	kJ/mol	39.3	0.7	MAP	13
E_{ki}	kJ/mol	44.1	0.7	MAP	13
E_{dis}	kJ/mol	55.4	0.2	MAP	13
5. Interstitial diffusion					
$E_{\text{diff,Si}}$	kJ/mol	73.6	0.3	MAP	27
$E_{\text{diff,B}}$	kJ/mol	34.6	0.4	MAP	13
6. Surface annihilation of interstitials					
S_{Si_i}	–	2.5×10^{-5}	§	§	25
S_{B_i}	–	2.5×10^{-5}	§	§	25

*Dissociation energies of intermediate clusters were determined by linear interpolation of ML estimates.
#ML estimation was based on only a single published value.
§Values of surface annihilation probability set based on experimental data in Ref. 25.

However, use of an effective annihilation probability fails to explain dopant pile-up[9] very near to the surface due to band bending. (We speculate that a variant of this effect may also contribute to the "uphill diffusion"[42] observed in solid-phase epitaxial regrowth.) Thus, band bending needs to be included in the simulations as a separate effect or qualitative effects may be missed. Surface interstitial annihilation[10] and near-surface band bending[26] are also separately sensitive to changes in surface treatment and annealing conditions. In this work, for example, we have argued that near-surface band bending operates during spike annealing but not soak annealing. A uniform incorporation of band bending (or neglect of it) under the two conditions leads to notably poorer agreement between simulations and experiments.

Figures 2 and 3 also show experimental and simulated values of the sheet resistance R_s. The revised model captures the qualitative trend in R_s, although there is a noticeable underestimate for spike annealing at 1000°C. We believe the discrepancy results primarily from the ML-based assumption of equal surface annihilation probabilities for boron and silicon ($S_{\text{B}_i} = S_{\text{Si}_i}$). These species may actually have different annihilation probabilities. Although S_{B_i} and S_{Si_i} should have similar effects on boron diffusion (where a high annihilation probability reduces profile spreading), they should have opposite effects on dopant activation. The sheet resistance R_s is related to the active dopant concentration C_s by[43]

$$R_s = \frac{1}{q\int_0^{x_j} \mu(x) C_s(x)\,dx}, \tag{9}$$

where q and μ are respectively the electron charge and the majority charge carrier mobility. The junction depth x_j is measured in this work at [B] = 5×10^{18} cm^{-3}. A high value of S_{Si_i} promotes the kick-in reaction in Eq. 2, which results in a higher C_s and a lower R_s. By contrast, a high S_{B_i} leads mainly to increased boron dose loss. The loss can lead to a lower C_s and a higher R_s. Direct measurement of S_{B_i} is needed to resolve the issue, though parameter sensitivity analysis on S_{B_i} and S_{Si_i} would help estimate the effects.

Improving the discretization of cluster energies is a model modification whose benefits are obvious: mitigation of the artificially discrete bursts of interstitial release as

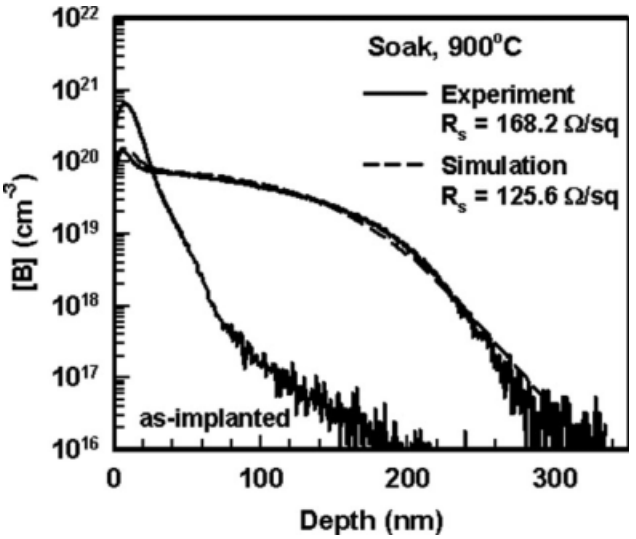

Figure 2. Experimental and simulated boron profiles for a soak anneal at 900°C for 1 h.

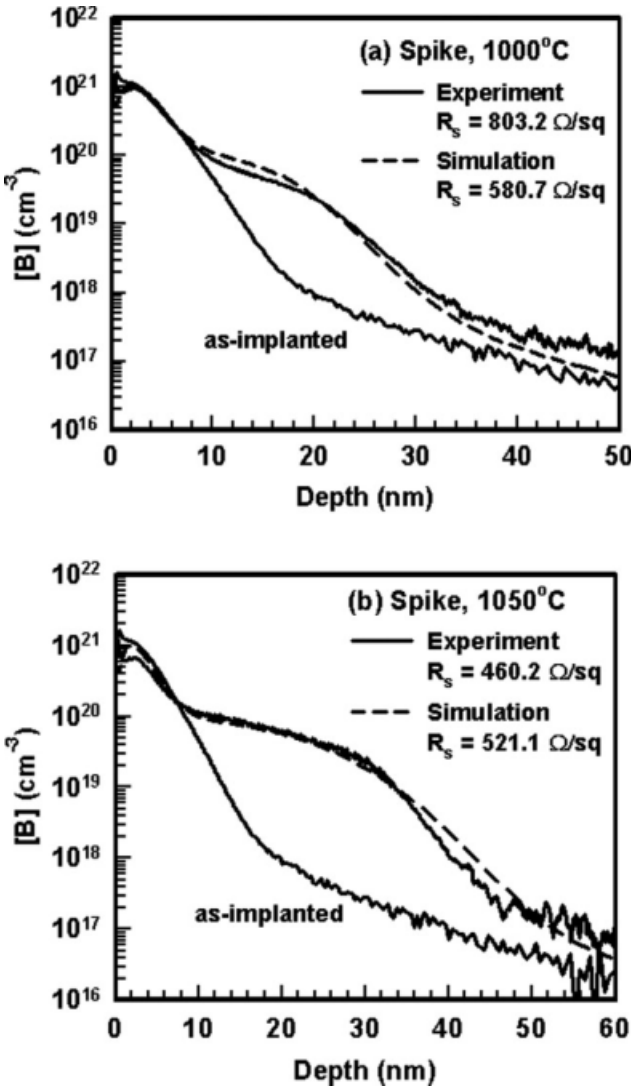

Figure 3. Experimental and simulated boron profiles for spike anneal with a peak temperature of (a) 1000°C and (b) 1050°C, respectively.

temperature increases. Yet the dissociation energy of mixed Si–B clusters still rises in discrete intervals of 34 kJ/mol (0.35 eV) for each atom added to a cluster, whereas the true variation of dissociation energy with cluster size is closer to a continuum.[28] The residual discretization could still lead to spurious effects in the sheet resistance (and doping profiles), although we believe these effects are likely to be small compared to surface effects.

Conclusion

We have presented a model for the diffusion and activation of implanted boron during thermal annealing that incorporates a newly discovered representation of surface annihilation of interstitials and near-surface band bending, together with refined cluster energetics. The model simulates boron diffusion over a wider range of annealing conditions than previous versions. This improved representation of dopant interaction with the surface and implant-induced defects is essential for explaining and predicting the behavior of complicated phenomena such as dopant pile-up near surfaces. Such an ability should prove useful in modeling millisecond annealing technologies.[12,44]

Acknowledgments

This work was partially supported by ACS Petroleum Research Fund (43651-AC5) and NSF (DMR 07-04354). SIMS for the soak-annealed material was performed at the Center for Microanalysis of Materials, University of Illinois, which is partially supported by the U. S. Department of Energy under grant DEFG02-96-ER45439. We thank Chris Hatem of Varian, Inc. for providing the boron-implanted wafer used for soak annealing.

Literature Cited

1. The International Technology Roadmap for Semiconductors, 2006. Available at: http://www.itrs.net/Links/2006update/2006UpdateFinal.htm
2. Aboy M, Pelaz L, López P, Marqués LA, Duffy R, Venezia VC. Physical insight into boron activation and redistribution during annealing after low-temperature solid phase epitaxial regrowth. *Appl Phys Lett*. 2006;88:191917.
3. Agarwal A, Gossmann H-J, Fiory AT. Effect of ramp rates during rapid thermal annealing of ion implanted boron for formation of ultra-shallow junctions. *J Electron Mater*. 1999;28:1333.
4. Gebel T, Voelskow M, Skorupa W, Mannino G, Privitera V, Priolo F, Napolitani E, Canera A. Flash lamp annealing with millisecond pulses for ultra-shallow boron profiles in silicon. *Nucl Instrum Methods Phys Res B*. 2002;186:287.
5. Chong YF, Pey KL, Wee ATS, See A, Tung C-H, Gopalakrishnan R, Lu YF. Application of excimer laser annealing in the formation of ultrashallow p+/n junctions. *Adv Microelectronic Process Tech*. 2000;4227:124.
6. Mokhberi A, Griffin PB, Plummer JD, Paton E, McCoy S, Elliott K. A comparative study of dopant activation in boron, BF_2, arsenic, and phosphorus implanted silicon. *IEEE Trans Electron Devices*. 2002;49:1183.
7. Poon CH, Tan LS, Cho BJ, See A, Bhat M. Boron profile narrowing in laser-processed silicon after rapid thermal anneal. *J Electrochem Soc*. 2004;151:G80.
8. Skorupa W, Gebel T, Yankov RA, Paul S, Lerch W, Downey DF, Arevalo EA. Advanced thermal processing of ultrashallow implanted junctions using flash lamp annealing. *J Electrochem Soc*. 2005;152:G436.
9. Jung MYL, Gunawan R, Braatz RD, Seebauer EG. Effect of near-surface band bending on dopant profiles in ion-implanted silicon. *J Appl Phys*. 2004;95:1134.
10. Seebauer EG, Dev K, Jung MYL, Vaidyanathan R, Kwok CTM, Ager JW, Haller EE, Braatz RD. Control of defect concentrations within a semiconductor through adsorption. *Phys Rev Lett*. 2006;97:055053.
11. Mendicino MA, Seebauer EG. Adsorption of $TiCl_4$ on Si(100). *Surf Sci*. 1992;277:89.
12. Lerch W, Paul S, Niess J, McCoy S, Selinger T, Gelpey J, Cristiano F, Severac F, Gavelle M, Boninelli S, Pichler P, Bolze D. Advanced activation of ultra-shallow junctions using flash-assisted RTP. *Mat Sci Eng B*. 2005;124-125:24.
13. Gunawan R, Jung MYL, Seebauer EG, Braatz RD. Maximum a posteriori estimation of transient enhanced diffusion energetics. *AIChE J*. 2003;49:2114.
14. Jung MYL, Gunawan R, Braatz RD, Seebauer EG. Ramp-rate effects on transient enhanced diffusion and dopant activation. *J Electrochem Soc*. 2003;150:G838.
15. Mark Law, University of Florida, Gainesville. Available at: http://www.swamp.tec.ufl.edu/.
16. Kirichenko TA, Banerjee S, Hwang GS. Surface chemistry effects on vacancy and interstitial annihilation on Si(001). *Phys Status Solidi B*. 2004;241:2303.

17. Kirchienko TA, Yu D, Sanjay SK, Banerjee K, Hwang GS. Silicon interstitials at Si/SiO_2 interfaces: density functional calculations. *Phys Rev B*. 2005;72:035345.
18. Crowder SW, Hsieh CJ, Griffin PB, Plummer JD. Effect of buried $Si-SiO_2$ interfaces on oxidation and implant-enhanced dopant diffusion in thin silicon-on-insulator film. *J Appl Phys*. 2004;76:2756.
19. Vuong H-H, Rafferty CS, Eshraghi SA, Ning J, McMacken JR, Chaudhry S, McKinley J, Stevie FA. Dopant dose loss at the $Si-SiO_2$ interface. *J Vac Sci Technol B*. 2000;18:428.
20. Lamrani Y, Cristiano F, Colombeau B, Scheid E, Calvo P, Schäfer H, Claverie A. Direct evidence of the recombination of silicon interstitial atoms at the silicon surface. *Nucl Instrum Methods Phys Res B*. 2004;216:281.
21. Lerch W, Stolwijk NA. Diffusion of gold in silicon during rapid thermal annealing: effectiveness of the surface as a sink for self-interstitials. *J Appl Phys*. 1998;83:1312.
22. Yeong SH, Srinivasan MP, Colombeau B, Chan L, Akkipeddi R, Kwok CTM, Vaidyanathan R, Seebauer EG. Defect engineering by surface chemical state in boron-doped preamorphized silicon. *Appl Phys Lett*. 2007;91:102112.
23. Vaidyanathan R, Seebauer EG, Graoui H, Foad MA. Influence of surface adsorption in improving ultrashallow junction formation. *Appl Phys Lett*. 2006;89:152114.
24. Kwok CTM, Dev K, Braatz RD, Seebauer EG. A method for quantifying annihilation rates of bulk point defects at surfaces. *J Appl Phys*. 2005;98:013524.
25. Dev K, Kwok CTM, Vaidyanathan R, Braatz RD, Seebauer EG. Controlling Dopant diffusion and activation through surface chemistry. Presented at: *Proceedings of 16th International Conference on Ion Implantation Technology*. 2006; 50.
26. Dev K, Jung MYL, Gunawan R, Braatz RD, Seebauer EG. Mechanism for coupling between properties of interfaces and bulk semiconductors. *Phys Rev B*. 2003;68:195311.
27. Kwok CTM, Dev K, Braatz RD, Seebauer EG. Maximum a posteriori estimation of activation energies that control silicon self-diffusion. *Automatica*. 2008;44:2241–2247.
28. Cowern NEB, Mannino G, Stolk PA, Roozeboom F, Huizing HGA, van Berkum JGM, Cristiano F, Claverie A, Jaraíz M. Energetics of self-interstitial clusters in Si. *Phys Rev Lett*. 1999;82:4460.
29. Caturla MJ, Foad M, Diaz de la Rubia T. The effect of ramp rate and annealing temperature on borontransient diffusion in implanted silicon: kinetic Monte Carlo simulations. Presented at*: Proceedings of 1998 International Conference on Ion Implantation Technology*. 1998;2:1018.
30. Kobayashi H, Nomachi I, Kusanagi S, Nishiyama F. Lattice site location of ultra-shallow implanted B in Si using ion beam analysis. *Mater Res Soc Symp Proc*. 2001;669:J 5.3.
31. Pelaz L, Aboy M, Lopez P, Marques LA. Atomistic modeling of dopant implantation, diffusion, and activation. *J Vac Sci Technol B*. 2006;24:2432.
32. Giles MD. Transient phosphorus diffusion below the amorphization threshold. *J Electrochem Soc*. 1991;138:1160.
33. Pelaz L, Gilmer GH,Gossmann H-J, Rafferty CS, Jaraiz M, Barbolla J. B cluster formation and dissolution in Si: a scenario based on atomistic modeling. *Appl Phys Lett*. 1999;74:3657.
34. Ortiz CJ, Pichler P, Fuhner T, Cristiano F, Colombeau B, Cowern NEB, Claverie A. A physically based model for the spatial and temporal evolution of self-interstitial agglomerates in ion-implanted silicon. *J Appl Phys*. 2004;96:4866.
35. Lee S, Hwang GS. Structure and stability of small compact self-interstitial clusters in crystalline silicon. *Phys Rev B*. 2008;77:085210.
36. Lee S, Hwang GS. Growth and shape transition of small silicon self-interstitial clusters. *Phys Rev B*. 2008;78:045204.
37. Gunawan R, Jung MYL, Braatz RD, Seebauer EG. Parameter sensitivity analysis applied to modeling transient enhanced diffusion and activation of boron in silicon. *J Electrochem Soc*. 2003;150:G758.
38. Beck JV, Arnold KY. *Parameter Estimation in Engineering and Science*. New York: Wiley, 1977.
39. Sparacino G, Tombolato C, Cobelli C. Maximum likelihood vs. maximum a posteriori parameter estimation of physiological system models: The C-peptide impulse response case study. *IEEE Trans Biomed Eng*. 2000;47:801.
40. Mannino G, Whelan S, Schroer E, Privitera V, Leveque P, Svensson BG, Napolitani E. An investigation on the modeling of transient enhanced diffusion of ultralow energy implanted boron in silicon. *J Appl Phys*. 2001;89:5381.
41. Ngau JL, Griffin PB, Plummer JD. Modeling the suppression of boron transient enhanced diffusion in silicon by substitutional carbon incorporation. *J Appl Phys*. 2001;90:1768.
42. Duffy R, Venezia VC, Heringa A, Hüsken TWT, Hopstaken MJP, Cowern NEB, Griffin PB, Wang CC. Boron uphill diffusion during ultrashallow junction formation. *Appl Phys Lett*. 2003;82:3647.
43. Cristiano F, Cherkashin N, Calvo P, Lamrani Y, Hebras X, Claverie A, Lerch W, Paul S. Thermal stability of boron electrical activation in preamorphised ultra-shallow junctions. *Mater Sci Eng B*. 2005; 114-115:174–179.
44. Baek S, Heo S, Choi H, Hwang H. Characteristics of heavily doped p^+/n ultrashallow junction prepared by plasma doping and laser annealing. *J Vac Sci Technol B*. 2005;23:257.

Manuscript received Dec. 8, 2008, and revision received May 26, 2009.